Chiral Supramolecular Organization from a Sheet-like Achiral Gel: Study of the Chiral Photoinduction†

Jorge Royes,[a] Víctor Polo,[b] Santiago Uriel,[c] Luis Oriol,[a] Milagros Piñol[a] and Rosa M. Tejedor*[d]

The chiral photoinduction in a photoresponsive gel based on an achiral 2D architecture with high geometric anisotropy and low roughness has been investigated. Circularly polarized light (CPL) was used as a chiral source and an azobenzene chromophore was employed as a chiral trigger. The chiral photoinduction was studied by evaluating the preferential excitation of enantiomeric conformers of the azobenzene units. Crystallographic data and density functional theory (DFT) calculations show how chirality is transferred to the achiral azomaterials as a result of the combination of chiral photochemistry and supramolecular interactions. This procedure could be applied to predict and estimate the chirality transfer from a chiral physical source to a supramolecular organization using different light-responsive units.

Introduction

The self-assembly of organic molecules to obtain well-defined supramolecular nanostructures is a multi-purpose tool in nanotechnology.[1,2] The supramolecular structures are defined by the number, orientation, strength and nature of intermolecular noncovalent interactions such as hydrogen bonding, halogen bonding, π-π stacking, dipole-dipole interactions and/or hydrophobic effects.[3,4]

Low molecular-weight organogels are amongst the most attractive supramolecular materials based on the well-defined self-assembly of the molecules.[5,6] In these systems, the inherent reversibility of the noncovalent interactions that maintain the supramolecular organization makes it possible to design materials that are sensitive to an external stimulus such as light or chemicals.[7-9] The gelator structure determines both gelator-gelator and gelator-solvent interactions and, as a consequence, the formation of the organogel, its supramolecular organization and the responsiveness of the final material are certainly controlled by the nature of the gelator.[10,11] Gels formed by photoresponsive gelators combine in the same material the thermal reversibility of the gel-sol transition with the control by light of the molecular packing. Azobenzenes, stilbenes, diarylethenes and spiropyrans are commonly used for this purpose.[10] Moreover, most of the examples are both hydro- and organogels based on photoresponsive gelators that exhibit fibrillar morphology[7,10,12] and only a few examples of gels with 2D structures have been described to date.[13-15]

Chiral physical forces can induce chiral supramolecular organization formed by achiral molecules.[16-18] The induction of chirality by light in achiral materials requires CPL as a chiral source and light-sensitive units to transmit the chiral information from light to the material.[19] In this context, it has been demonstrated that CPL irradiation of azobenzenes can induce chiral supramolecular arrangements of the azobenzene chromophores.[20] Furthermore, we reported chiral photoinduction by CPL in achiral liquid crystalline azomaterials[21-23] and even in achiral amorphous azopolymers.[24]

The preparation of shape-controlled nanoobjects based on organic materials is an advanced topic in supramolecular engineering.[25-29] In particular, nanosheets have opened up a wide range of potential technological applications in the fields of device fabrication, catalysis, sensing, separation, electronic, photoelectronic and biomaterials.[30] Building 2D architectures requires careful molecular design to promote 2D-directed cooperative intermolecular interactions.[31] The preparation of chiral nanosheets from achiral molecules is still unusual but interesting applications have been proposed for these chiral assemblies, e.g., chemical and biological detection, enantioselective synthesis, membrane-based chiral separation and molecular devices.[32]

The work described here concerns an organogel based on the achiral crown ether azobenzene gelator **12-AZO15/5** (Fig. 1). The morphology of the solid network of this photoresponsive gel has been investigated and crystallographic data and the DFT methodology were employed to study the transference of the chirality from the circularly polarized light to an achiral gel of **12-AZO15/5** to give a chiral material.

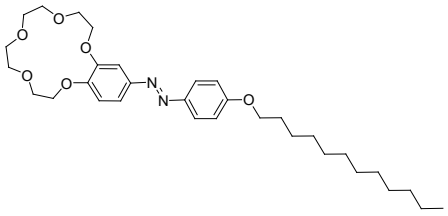

Fig. 1 The gelator 4'-(*p*-dodecyloxyphenylazo)benzo[15]crown-5 ether (**12-AZO15/5**).

Results and Discussion

Gelation behavior

The compound **12-AZO15/5** has been described previously[33,34] and the gelation ability and optical properties of selected gels of **12-AZO15/5** were reported. Details of the synthesis and characterization of gelators and instrument and methods used are provided in the Supporting Information. The gelation of organic solvents by low molecular weight compounds is often

illustrated by the ability to invert a test tube that contains the gelator and solvent without the sample flowing.[35,36] Using this criterion, the gelation capability of **12-AZO15/5** was first studied at room temperature in polar and nonpolar solvents at 5.0% wt concentration. In cases where a gel was formed, lower concentrations were tested in order to evaluate the minimum gelation concentration (MGC) at room temperature. **12-AZO15/5** gelled at room temperature in several of the solvents tested (Table S1 in the Supporting Information) to yield opaque gels that were stable for months without apparent phase separation. Gels in 1-dodecanol were selected for a more in-depth study because this solvent has a high boiling point and a relatively low vapor pressure.[37]

Gels in 1-dodecanol of **12-AZO15/5** showed different morphologies depending on the gelator concentration (Fig. 2). At levels below 3.0% wt of **12-AZO15/5** the gels exhibited a fibrillar morphology but above 5.0% wt the solid network of the gels was based on platelets. In the range between 3.0% and 5.0% wt both sheets and fibers were observed. To the naked eye the soft states organized in platelets are pearlescent, while the fibrillar gels had a matt appearance and looked more continuous than the sheet-like ones. The color of the gels depends on the morphology. The gels with the fibrillar morphology were yellow and the sheet-like gels were orange, which suggests that the aggregates of the azobenzene groups are different as UV-vis spectra indicate (Fig. S1 in the Supporting Information). G(12-AZO15/5)-2.0 and G(12-AZO15/5)-6.0 (Fig. 2) were selected for morphological and optical studies. However, it was observed that the formation of G(12-AZO15/5)-2.0 was controlled by the cooling rate of the initial solution. At a low cooling rate, 1 K min^{-1}, the gel was not obtained and **12-AZO15/5** precipitated as sheet-like crystals, but rapid cooling of the solution (>5 K min^{-1}) led to the formation of the fibrillar gel.[38] These results limited the study of G(12-AZO15/5)-2.0. Conversely, the formation of sheet-like G(12-AZO15/5)-6.0 was not dependent on the cooling rate. Both gels were birefringent (Fig. 2) and this is consistent with a well-defined molecular organization.

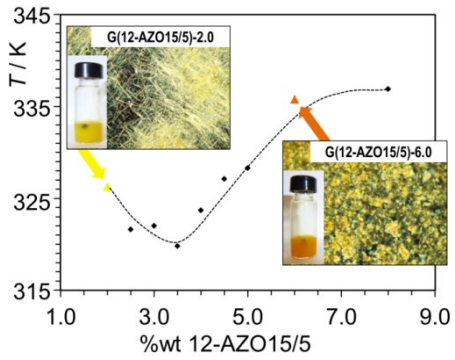

Fig. 2 Gel-sol temperature (T_{gel}, falling sphere test) *vs.* gelator concentration of **12-AZO15/5** gels in 1-dodecanol. Polarized optical microscopy (POM) images and macroscopic aspect of G(12-AZO15/5)-2.0 and G(12-AZO15/5)-6.0.

Gel-sol transition temperatures of the **12-AZO15/5** gels, as determined by the dropping ball method (T_{gel}), decreased slightly from 2.0 to 3.5% wt and increased at concentrations above 3.5% wt with an exponential relationship observed (Fig. 2). This unusual behavior of the **12-AZO15/5** gels is related to the two different morphologies observed by POM.[39,40]

Morphology studies

The results of the POM study indicated that the morphology of the **12-AZO15/5** gels depends on the gelator concentration. In fact, the images obtained by scanning electron microscopy (SEM) of the xerogel from G(12-AZO15/5)-2.0 showed a network of entangled thin, flexible and uniform fibers (Fig. 3a). However, the SEM images of the G(12-AZO15/5)-6.0 xerogel (Fig. 3b) revealed a completely different morphology, as the gel-like state arises from a dense aggregation of irregular thin sheets. Cryogenic scanning electron microscopy (cryo-SEM) was used to obtain further insights into the gel structure (Fig. 3c and 3d). The cryo-SEM images proved that the xerogels retain the gel structure and they also confirmed the influence of the **12-AZO15/5** concentration on the gel morphology.

The sheet thickness and surface roughness of sheet-like G(12-AZO15/5)-6.0 were determined by atomic-force microscopy (AFM) (Fig. 4). The measured sheet thickness was 3.9±0.8 nm and the histogram indicates a uniform sheet thickness. Moreover, the AFM measurements suggest that the surfaces of the sheets are extremely smooth. In fact, the root mean square values (R_{RMS}) for the surface roughness measured at various zones of the plates were in the range 0.3–0.4 nm.[41] These results indicate that the solid networks of the 1-dodecanol gel are formed by low-roughness nanosheets.[42]

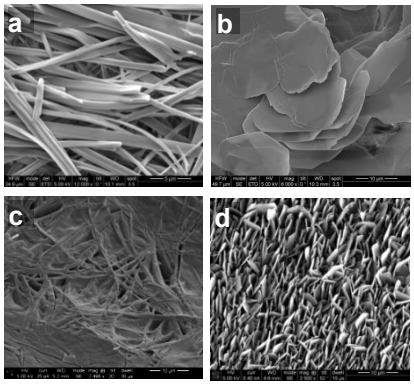

Fig. 3 Xerogels from G(12-AZO15/5)-2.0 and G(12-AZO15/5)-6.0: SEM images (a and b, respectively) and cryo-SEM images (c and d, respectively).

X-ray diffraction and molecular packing model

The X-ray diffraction (XRD) diagrams for G(12-AZO15/5)-6.0 and a polycrystalline sample of the gelator were recorded at room temperature (Fig. 5). The XRD patterns of the gel showed diffraction peaks due to (0 0 n) consistent with a lamellar structure. The layer *d*-spacing in the sheets of G(12-AZO15/5)-6.0 was 38 Å. These data are consistent with the minimum layer thicknesses determined by AFM. Moreover, the calculated molecular length of the gelator **12-AZO15/5** is 32 Å. Given this value, the layer of **12-AZO15/5** could be formed by tilted dimers. The fibrillar xerogel formed by G(12-AZO15/5)-2.0 did not show typical diffraction peaks of a crystalline material (Fig. S2 in the Supporting Information) and this finding could be due to the aggregates being less regular than the sheet-like structure.[43]

According to the XRD results, the solid network of G(12-AZO15/5)-6.0 retains a certain degree of crystallinity (Fig. 5). Therefore, the platelet gelled state can be described as lamellar aggregates with a molecular packing order quite similar to the crystalline solid.[44] In cases where the XRD pattern of the gel and crystalline sample of the gelator are similar, an accurate model for the molecular packing in the xerogel can be obtained from the crystalline structure in the bulk single crystal.[1,2,37,44] Unfortunately, the crystalline structure of **12-AZO15/5** could not be determined. For this reason, the model compound **1-AZO15/5** (Fig. 6), which contains a methoxy terminal group instead of the dodecyloxy group in **12-AZO15/5**, was synthesized and its crystal structure was resolved (see Supporting Information). Although the gelation ability of **1-AZO15/5** (Table S1 in the Supporting Information) was not as good as that of **12-AZO15/5**, the model compound fortunately gelled with dodecane and 1-dodecanol. This allowed an investigation into the corresponding gel G(1-AZO15/5)-5.0 (1-dodecanol gel, MGC 5.0% wt). The SEM analysis confirmed that the xerogel formed by G(1-AZO15/5)-5.0 had a sheet-like morphology (Fig. 6a) similar to that exhibited by G(12-AZO15/5)-6.0. The powder XRD patterns of the G(1-AZO15/5)-5.0 gel and the polycrystalline sample were registered and these proved that a lamellar organization with a *d*-spacing about 2.8 nm was present (Fig. 6b). Furthermore, the AFM study revealed that the nanosheet thickness is 2.6±0.4 nm (Fig. S3 in the Supporting Information).

1-AZO15/5 crystallizes in the monoclinic $P2_1/c$ space group[45] (see the Supporting Information). The molecules of **1-AZO15/5** form dimers due to weak hydrogen bonds C(1)-H···O(1) [2.60(4) Å, 148(3)°] between the methoxy groups (Fig. 6c). The dimers are arranged in a herringbone-type packing (70.5°) along the *b* axis, thus giving rise to layers with a width of 23.2 Å due to the tilt of dimers, which measure approximately 34 Å. This crystal structure is consistent with the arrangement of the gelators in the solid networks of the gels. The *d*-spacing of the layers corresponds to the nanosheet thickness measured by AFM. The polarizing optical microscopy study showed that the individual platelets are birefringent at an orthogonal angle and this result supports the proposed model based on the gelator molecules being titled with respect to the sheet surfaces.[37]

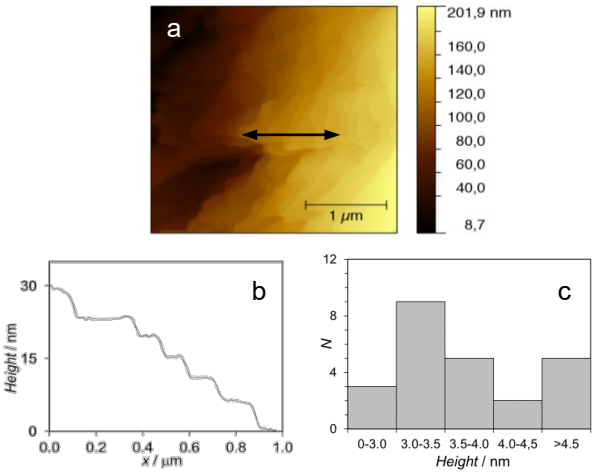

Fig. 4 AFM data of xerogel from G(12-AZO15/5)-6.0: (a) AFM height image; (b) cross-section profiles of xerogel, and (c) step-height distribution histograms.

On the basis of the results discussed above it seems reasonable to propose that the nanosheets of G(12-AZO15/5)-6.0 consist of tilted dimers of **12-AZO15/5** in a similar way to the model compound **1-AZO15/5**. According to the proposed model for the molecular packing in G(12-AZO15/5)-6.0, the crown ether moieties should point to the sheet surface and the aliphatic chains would be packed inside the nanosheets. Therefore, the sheet surface should be hydrophilic. In order to verify this proposal, the hydrophilicity of the xerogel from G(12-AZO15/5)-6.0 was characterized by measuring the water contact angle (CA) at its surface. The CA on the xerogel formed by G(12-AZO15/5)-6.0 was 58.1±1.4° (Fig. S4 in the Supporting Information), which seems to confirm the proposed molecular assembly based on tilted dimers with the hydrophilic units (crown ether units) pointing outwards from the sheet surface.

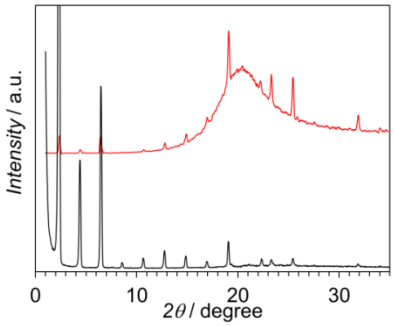

Fig. 5 Powder XRD diagrams of G(12-AZO15/5)-6.0 (red) and polycrystalline **12-AZO15/5** (black).

Chiral photoinduction

The absorption spectrum of **12-AZO15/5** in 1-dodecanol solution displayed the characteristic absorption bands of the azobenzene chromophores (Fig. 7a). The absorption maximum corresponds to the π-π* transition with the transition moment parallel to the long axis of the azo chromophore. The less intense band at around 450 nm is due to the n-π* transition. The π-π* transition with the transition moment parallel to the short axis of the *E*-azobenzene units was observed at around 250 nm. The gel showed more complex, red-shifted and broader π-π* transition bands, which suggests the presence of aggregates in which the azobenzene units are tilted (J aggregates).[46] In fact, the proposed model for the solid network that supports the gels points to J-aggregation of the azo chromophores into the nanosheets. Kondo *et al*. reported a similar crystalline structure consisting of stacks of monolayer J-aggregates of symmetric azocompounds that form plate-like crystals.[47-49] Moreover, the platelets of these compounds show specular reflectance and a flat surface similar to the solid network of G(12-AZO15/5)-6.0.

The photoinduction of chirality in gels was evaluated by electronic circular dichroism (ECD). Spectra were registered before and five minutes after irradiation with CPL. Before irradiation the gels were ECD silent, which confirmed an achiral material. As discussed above, the fibrillar gel G(12-AZO15/5)-2.0 corresponds to a metastable state and it was not possible with the available experimental data to propose a molecular packing model for this gel morphology. For this reason, the irradiation of G(12-AZO15/5)-2.0 was not carried out.

A preliminary study was carried out to establish the optimum irradiation conditions for G(12-AZO15/5)-6.0. The gel was irradiated with CPL at 365 or 488 nm (Fig. S5 in the Supporting Information shows UV-vis of G(12-AZO15/5)-6.0 after CPL irradiation), which correspond to π–π* and n-π* transitions, respectively. Irradiation at 365 nm (CPL) quickly gave rise to a gel-sol transition due to the trans-cis photoisomerization and chiral photoinduction was not detected under these irradiations conditions, even before the photoinduced gel-sol transition. Conversely, net ECD spectra were registered after irradiation with *left*- or *right*-CPL (*l*-CPL or *r*-CPL) at 488 nm (Ar^+ laser, 25 mW/cm^2). Moreover, at this wavelength the chiroptical response increased with the irradiation time up to 80 minutes without detecting gel-sol transition (Fig. S6 in the Supporting Information). Therefore, according to these results the gel was irradiated with *l*-CPL or *r*-CPL at 488 nm for 80 minutes and it was confirmed that the gel state was retained. After CPL irradiation under these conditions, the gel exhibited a clear chiroptical response (Fig. 7b) and changes in the UV-vis spectra were not observed. The photoinduced ECD spectra showed an exciton couplet associated with the main absorption and a less intense couplet corresponding to the π–π* transition moment parallel to the short axis of the azobenzene units. Moreover, the opposite ECD spectrum was obtained when CPL with the opposite handedness was applied. This chiral response has been ascribed to chiral aggregates in which the azobenzene units have a prevailing handedness.[22,23,50] Unfortunately, irradiation of G(1-AZO15/5)-5.0 could not be carried out because a gel-sol transition was detected before irradiation could be carried out when the gel was placed in cell. This finding could be due to the poor gelation ability of **1-AZO15/5**.

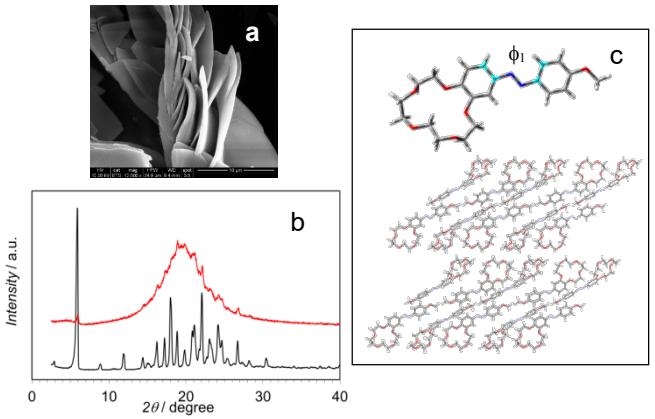

Fig. 6 (a) SEM image of the xerogel formed by G(1-AZO15/5)-5.0; (b) powder XRD diagrams of G(1-AZO15/5)-5.0 (red) and polycrystalline **1-AZO15/5** (black), and (c) crystalline structure of **1-AZO15/5**.

A key issue concerning this photoinduction of chiroptical properties in gel materials is how the CPL generates net chirality. The crystallographic structure of **1-AZO15/5**

confirmed that the preferred conformation of the azobenzene units in the crystal is not fully planar, with a torsion angle defined by C(9)–C(8)–C(5)–C(4) (ϕ_1) of 6°, as shown in Fig. 6. Consequently, the benzene ring of the benzo[15]crown-5 ether unit is not coplanar with the phenylazo unit and this results in chiral conformations of the gelator. Based on the structural similarities with the crystalline structure, it is reasonable to propose that nonplanar conformers can be present in the solid network of G(12-AZO15/5)-6.0. The presence of nonplanar conformations of azobenzene units has been confirmed in some systems.[51,52] Indeed, the irradiation with CPL of stable enantiomers of *E* azobenzene derivatives can induce an enantiomeric excess caused by a preferential interaction of one of the *E*-enantiomers with *l*- or *r*-CPL.[53,54]

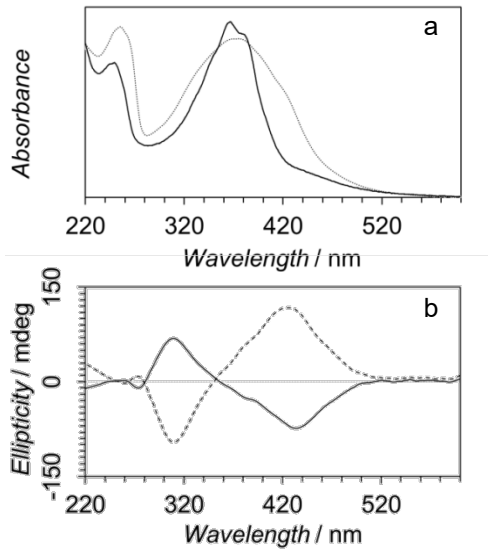

Fig. 7 (a) UV-vis absorption spectra of **12-AZO15/5** in 1-dodecanol solution (—) and G(12-AZO15/5)-6.0 (—), and (b) electronic circular dichroism (ECD) spectra of *right*-CPL (*r*-CPL, --) and *left*-CPL (*l*-CPL,—) irradiated samples of G(12-AZO15/5)-6.0 for 80 min (488 nm Ar^+ line, 25 mW/cm^2).

With the aim of explaining the chiral photoinduction in the achiral gel, our approach is based on the asymmetric induction by preferential excitation of enantiomeric conformers in the racemic mixture of the photoactive gelators using *l*- or *r*-CPL.[55] The anisotropy factor, *g* factor,[56-58] defined as the normalized difference in the molar extinction coefficients between optically pure isomers toward *l*- or *r*-CPL at a given wavelength, regulates the degree of preferential excitation by CPL and, consequently, the photoinduced enantiomeric excess.[58,59] In order to evaluate the *g* factor for the molecular structure with slight distortions in the angle between the benzene rings (ϕ_1) and thus validate our hypothesis, we conducted a theoretical study using the time-dependent density functional theory (TD-DFT) methodology to calculate the UV-vis and ECD spectra.

Firstly, in order to adjust the method, the UV-vis and ECD spectra of the enantiomers in the crystal structure of the *E* isomer for **1-AZO15/5** were calculated at the TD-B3LYP-D3/6-31G(d) level with Gaussian 09[60] for gas phase and in 1-octanol solution using the polarizable continuous model (PCM) approach. The obtained results *in vacuo* are in good agreement with the registered UV-vis spectra of 1-dodecanol solutions of **1-AZO15/5** and **12-AZO15/5** (Fig. S7 in the Supporting Information). Considering the calculated UV-vis and ECD spectra, we estimated the *g* factor at different wavelengths. The UV-vis and ECD spectra are shown in Fig. 8 along with the *g* factor calculated for a selected chiral *E* isomer of **1-AZO15/5** in the crystalline structure. The calculated ECD spectrum showed a positive Cotton effect corresponding to the $\pi-\pi^*$ transition and a negative Cotton effect for the forbidden n-π^* transition. Both Cotton effects for **1-AZO15/5** have similar ECD absolute values. The *g* factors at 365 and 488 nm are $1.40\cdot10^{-4}$ and $4.40\cdot10^{-3}$, respectively, and these are typical values for aromatic compounds.[61] Moreover, it is worth highlighting that the anisotropy factor corresponding to the partially forbidden n-π^* transition is higher than the *g* factor at 365 nm close to the $\pi-\pi^*$ transition. Secondly, the geometrical parameters of **12-AZO15/5** *in vacuo* (starting from the **1-AZO15/5** crystalline structure) were optimized by DFT calculations at the B3LYP-D3/6-31G(d) level. The angle ϕ_1 (Fig. 9) in the optimized conformation of **12-AZO15/5** was 1.6°. This optimized geometry was used to calculate the UV-vis and ECD spectra from 200 to 700 nm by the TD-DFT methodology and the *g* factor at 488 nm of the optimized structure was $1.20\cdot10^{-3}$.

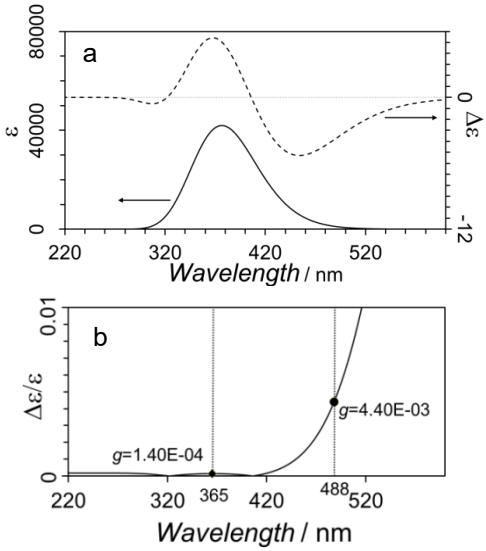

Fig. 8 (a) UV and ECD spectra calculated by the TD-DFT methodology for a selected chiral *E* isomer of **1-AZO15/5** for the crystalline structures and (b) calculated *g* factor for the chiral structure of **1-AZO15/5** *vs.* wavelength.

Finally, the dependence of the energy, relative to the optimized structure of **12-AZO15/5**, with regard to ϕ_1 was analyzed using partial optimizations, with all of the remaining geometrical variables relaxed. The potential energy scans were performed by varying ϕ_1 from the optimum value in steps of 1° up to 19.6° (1.6°+18×1°). The UV and ECD spectra (Fig. 9a and 9b) and the *g* factor at 488 nm were then calculated for each increment of ϕ_1. The variation of the energy and the *g* factor at 488 nm *vs* ϕ_1 for **12-AZO15/5** is represented in Fig. 9c. As expected, the energy increased with ϕ_1, but in the range from 1.6° to 19.6° the energetic barrier was below 1.5 kJ mol^{-1}. The torsion of the benzene rings along the N–N axis up to 19.6° is allowed under the current experimental conditions.[62]

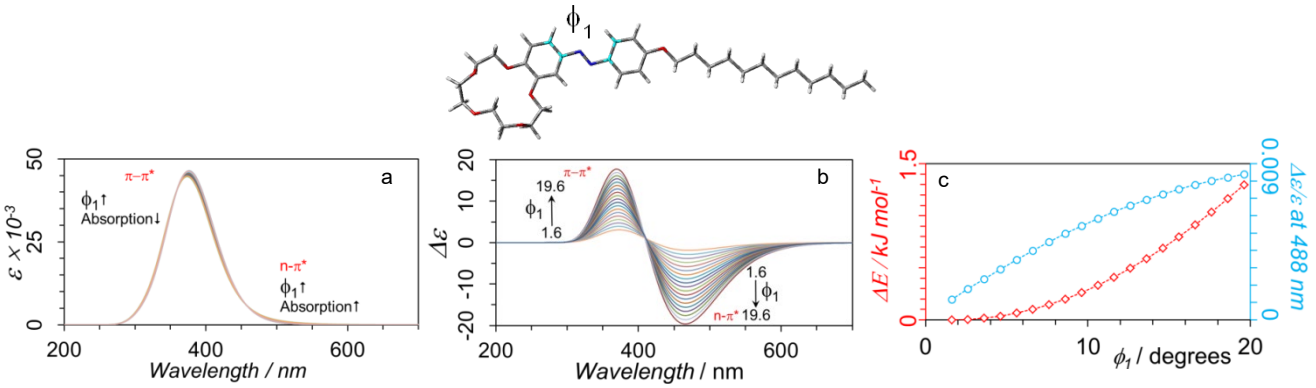

Fig. 9 Calculated absorption (a) and ECD spectra (b) of **12-AZO15/5** on modifying ϕ_1. TD-DFT method at the B3LYP-D3-6-31G* level Gaussian 09. (c) The relative energy of the conformers of **12-AZO15/5** and the *g* factor at 488 nm *vs* ϕ_1 for **12-AZO15/5**.

The supramolecular interactions that support the solid network of G(12-AZO15/5)-6.0 may prefer a slightly non-planar conformation, as occurs in the crystalline structure of **1-AZO15/5**, and the solid matrix may freeze the rotation of the benzene ring along the N–N axis. As the non-planar conformer is chiral, prior to CPL irradiation the solid network must be formed by a racemic mixture of enantiomeric conformers and aggregates. Otherwise, the *g* factor at 488 nm, and consequently the degree of preferential excitation on using *l*- or *r*-CPL, would increase with ϕ_1. In fact, at 488 nm a variation of three degrees of ϕ_1 in the minimum energy structure leads to an increase in the *g* factor from 0.001 to 0.003. This noteworthy increase in the *g* factor due to slight modifications of ϕ_1 is achievable with an energy cost of around 0.04 kJ/mol according to the DFT data. The effective supramolecular interactions impose a high conformational restriction that avoids the rotation of the benzene units and fixes the chiral conformers. CPL irradiation yields bent *Z* isomers and these have a less appropriate structure to establish supramolecular interactions, e.g. π–π stacking, and a higher dipolar moment that can increase the solubility with respect to the *E* isomer. Both factors can allow a fast ground state racemization of the *Z* isomers. Finally, the *E-Z-E* cycles induced by 488 nm CPL are able to enrich one of the *E* enantiomeric conformers. According to the majority rule principle,[63] a strong bias towards the chiral organization preferred by the major enantiomer can be achieved through supramolecular interactions and this results in an excess of one of the chiral aggregates.[64,65] The ECD of the CPL-irradiated gel corresponds to the chiral aggregates imposed by the major *E* conformer. Irradiation with CPL of opposite handedness led to an enantiomeric excess of the other chiral conformer and consequently an opposite ECD signal due to the enantiomeric aggregates.

Conclusions

Photoresponsive achiral gels supported by a 2D layer nanostructure have been prepared and a new class of chiral material has been obtained by CPL irradiation of the achiral gel. This chiral photoinduction is based on the preferential excitation of nonplanar conformers of the azogelator. Moreover, the presence of these nonplanar conformations has been proven by the crystallographic data from a crystalline model compound and by DFT calculations. Furthermore, the anisotropy factor of nonplanar conformers calculated in a theoretical study using the TD-DFT methodology to calculate UV-vis and ECD spectra proved to be a useful parameter to evaluate the effectiveness of the chiral photoinduction in an achiral material. In summary, we have carried out an in-depth study into the transformation of achiral supramolecular structures in chiral supramolecular material based on conformational chirality. It was concluded that a combination of crystallographic data and DFT calculations provides good evidence to explain how chirality is transferred to the materials. This method could be used to evaluate the chiral photoinduction using other chiral triggers.

Acknowledgements

This work was supported by the Ministerio de Economía y Competitividad, under the project MAT2014-55205-P, Fondo Europeo de Desarrollo Regional (FEDER) and Gobierno de Aragón. The authors acknowledge the Laboratory of Advanced Microscopy Laboratory (LMA) of the Universidad de Zaragoza (Unizar) and CEQMA (CSIC-Unizar) for the NMR, MS, EA and thermal analysis general facilities. The authors additionally acknowledge the use of the Servicio General de Apoyo a la Investigación of the Universidad de Zaragoza. General Research Services SGIker technical support from UPV/EHU

(MEC, GV/EJ, European Social Fund) is gratefully acknowledged.

1 J. L. Atwood and J. W. Steed, *Organic Nanostructures*, Wiley-VCH, Weinheim, 2008.

2 J. M. Lehn, *Supramolecur Chemistry*, Wiley-VCH, Weinheim, 1995.

3 K. Ariga, H. Ito, J. P. Hill and H. Tsukube, *Chem. Soc. Rev.*, 2012, **41**, 5800-5835.

4 K. J. M. Bishop, C. E. Wilmer, S. Soh and B. A. Grzybowski, *Small*, 2009, **5**, 1600-1630.

5 P. Terech and R. G. Weiss, *Chem. Rev.*, 1997, **97**, 3133-3159.

6 G. Yu, X. Yan, C. Han and F. Huang, *Chem. Soc. Rev.*, 2013, **42**, 6697-6722.

7 N. M. Sangeetha and U. Maitra, *Chem. Soc. Rev.*, 2005, **34**, 821-836.

8 X. Yang, G. Zhang and D. Zhang, *J. Mater. Chem.*, 2012, **22**, 38-50.

9 S. Ghosh, V. K. Praveen and A. Ajayaghosh, *Ann. Rev. Mater. Res.,* 2016, **46**, 235-262.

10 S. S. Babu, V. K. Praveen and A. Ajayaghosh, *Chem. Rev.*, 2014, **114**, 1973-2129.

11 V. K. Praveen, C. Ranjith and N. Armaroli, *Angew. Chem. Int. Ed.*, 2014, **53**, 365-368.

12 A. Gopal, M. Hifsudheen, S. Furumi, M. Takeuchi and A. Ajayaghosh, *Angew. Chem. Int. Ed.*, 2012, **51**, 10505-10509.

13 J. H. Jung, Y. Ono and S. Shinkai, *Langmuir*, 1999, **16**, 1643-1649.

14 J. H. Jung, H. Kobayashi, M. Masuda, T. Shimizu and S. Shinkai, *J. Am. Chem. Soc.*, 2001, **123**, 8785-8789.

15 Y. Zhou, T. Yi, T. Li, Z. Zhou, F. Li, W. Huang and C. Huang, *Chem. Mater.*, 2006, **18**, 2974-2981.

16 M. Avalos, R. Babiano, P. Cintas, J. L. Jimenez, J. C. Palacios and L. D. Barron, *Chem. Rev.*, 1998, **98**, 2391-2404.

17 M. Liu, L. Zhang and T. Wang, *Chem. Rev.*, 2015, **115**, 7304-7397.

18 E. Yashima, N. Ousaka, D. Taura, K. Shimomura, T. Ikai and K. Maeda, *Chem. Rev.*, 2016, **116**, 13752-13990.

19 R. M. Tejedor, L. Oriol, J. L. Serrano and T. Sierra, *J. Mater. Chem.*, 2008, **18**, 2899-2908.

20 S. W. Choi, S. Kawauchi, N. Y. Ha and H. Takezoe, *Phys. Chem. Chem. Phys.*, 2007, **9**, 3671-3681.

21 J. Royes, J. Rebolé, L. Custardoy, N. Gimeno, L. Oriol, R. M. Tejedor and M. Piñol, *J. Polym. Sci., Part A: Polym. Chem.*, 2012, **50**, 1579-1590.

22 R. M. Tejedor, M. Millaruelo, L. Oriol, J. L. Serrano, R. Alcala, F. J. Rodriguez and B. Villacampa, *J. Mater. Chem.*, 2006, **16**, 1674-1680.

23 R. M. Tejedor, L. Oriol, J. L. Serrano, F. Partal Ureña and J. J. López González, *Adv. Funct. Mater.*, 2007, **17**, 3486-3492.

24 J. Royes, C. Provenzano, P. Pagliusi, R. M. Tejedor, M. Pinol and L. Oriol, *Macromol. Rapid Commun.*, 2014, **35**, 1890-1895.

25 N. Chandrasekhar and R. Chandrasekar, *Angew. Chem. Int. Ed.*, 2012, **51**, 3556-3561.

26 Y.-b. Lim, K.-S. Moon and M. Lee, *Chem. Soc. Rev.*, 2009, **38**, 925-934.

27 S. Mahesh, A. Gopal, R. Thirumalai and A. Ajayaghosh, *J. Am. Chem. Soc.*, 2012, **134**, 7227-7230.

28 R. Rajaganesh, A. Gopal, T. Mohan Das and A. Ajayaghosh, *Org. Lett.*, 2012, **14**, 748-751.

29 R. D. Mukhopadhyay, V. K. Praveen and A. Ajayaghosh, *Materials Horizons*, 2014, **1**, 572-576.

30 T. Govindaraju and M. B. Avinash, *Nanoscale*, 2012, **4**, 6102-6117.

31 S.-L. Cai, W.-G. Zhang, R. N. Zuckermann, Z.-T. Li, X. Zhao and Y. Liu, *Adv. Mater.*, 2015, **27**, 5762-5770.

32 X. Hou, M. Schober and Q. Chu, *Cryst. Growth Des.*, 2012, **12**, 5159-5163.

33 K. L. Genson, D. Vaknin, O. Villacencio, D. V. McGrath and V. V. Tsukruk, *J. Phys. Chem. B*, 2002, **106**, 11277-11284.

34 K. Larson, D. Vaknin, O. Villavicencio, D. McGrath and V. V. Tsukruk, *J. Phys. Chem. B*, 2002, **106**, 7246-7251.

35 C. Macosko, *Rheology: Principles, Measurements and Applications*, VCH Published, 1994.

36 S. R. Raghavan and B. H. Cipriano, in *Molecular Gels. Materials with seft-Assemble Fibrillar Networks*, eds. R. G. Weiss and P. Terech, Dordrecht, 2006, ch. 8, pp. 241-252.

37 D. J. Abdallah, S. A. Sirchio and R. G. Weiss, *Langmuir*, 2000, **16**, 7558-7561.

38 L. Zhang, X. Wang, T. Wang and M. Liu, *Small*, 2015, **11**, 1025-1038.

39 K. Murata, M. Aoki, T. Suzuki, T. Harada, H. Kawabata, T. Komori, F. Ohseto, K. Ueda and S. Shinkai, *J. Am. Chem. Soc.*, 1994, **116**, 6664-6676.

40 V. J. Nebot, J. Armengol, J. Smets, S. F. Prieto, B. Escuder and J. F. Miravet, *Chem. Eur. J.*, 2012, **18**, 4063-4072.

41 E. S. Gadelmawla, M. M. Koura, T. M. A. Maksoud, I. M. Elewa and H. H. Soliman, *J. Mater. Process. Technol.*, 2002, **123**, 133-145.

42 R. Davis, R. Berger and R. Zentel, *Adv. Mater.*, 2007, **19**, 3878-3881.

43 Y. Wu, S. Wu, G. Zou and Q. Zhang, *Soft Matter*, 2011, **7**, 9177-9183.

44 E. Ostuni, P. Kamaras and R. G. Weiss, *Angew. Chem. Int. Ed.*, 1996, **35**, 1324-1326.

45 *Crystallographic data (excluding structure factors) for the structure(s) reported in this paper have been deposited with the Cambridge Crystallographic Data Centre as supplementary publication no. CCDC-1516204 Copies of the data can be obtained free of charge from www.ccdc.cam.ac.uk/conts/retrieving.html*.

46 M. Kasha, H. R. Rawls and M. A. El-Bayoumi, *Pure Appl. Chem.*, 1965, **11**, 371-392.

47 A. Matsumoto, M. Kawaharazuka, Y. Takahashi, N. Yoshino, T. Kawai and Y. Kondo, *J. Oleo Sci.*, 2010, **59**, 151-156.

48 Y. Kondo, A. Matsumoto, K. Fukuyasu, K. Nakajima and Y. Takahashi, *Langmuir*, 2014, **30**, 4422-4426.

49 Y. Kondo, K. Nakayima, M. Kato, H. Ohrui and A. Takahashi, *Color. Technol.*, 2015, **131**, 255-258.

50 G. Iftime, F. L. Labarthet, A. Natansohn and P. Rochon, *J. Am. Chem. Soc.*, 2000, **122**, 12646-12650.

51 M. J. Comstock, D. A. Strubbe, L. Berbil-Bautista, N. Levy, J. Cho, D. Poulsen, J. M. J. Fréchet, S. G. Louie and M. F. Crommie, *Phys. Rev. Lett.*, 2010, **104**, 178301.

52 N. O. Iskeleli, H. Karabiyik, C. Albayrak, E. Agar and I. E. Gumrukcuoglu, *Struct. Chem.*, 2008, **19**, 565-570.

53 P. K. Hashim, R. Thomas and N. Tamaoki, *Chem. Eur. J.*, 2011, **17**, 7304-7312.
54 S.-W. Choi and H. Takezoe, *Soft Matter*, 2016, **12**, 7937-7942.
55 A. Steinbacher, P. Nuernberger and T. Brixner, *Phys. Chem. Chem. Phys.*, 2015, **17**, 6340-6346.
56 W. Kuhn, *Trans. Faraday Soc.*, 1930, **26**, 0293-0307.
57 W. Kuhn and E. Knopf, *Z. Phys. Chem.*, 1930, **7**, 292-310.
58 H. Rau, *Chiral Photochemistry*, Marcel Dekker, New York, 2004.
59 K. Rijeesh, P. K. Hashim, S.-i. Noro and N. Tamaoki, *Chem. Sci.*, 2015, **6**, 973-980.
60 M. J. Frisch, G. W. Trucks, H. B. Schlegel, G. E. Scuseria, M. A. Robb, J. R. Cheeseman, G. Scalmani, V. Barone, B. Mennucci, G. A. Petersson, H. Nakatsuji, M. Caricato, X. Li, H. P. Hratchian, A. F. Izmaylov, J. Bloino, G. Zheng, J. L. Sonnenberg, M. Hada, M. Ehara, K. Toyota, R. Fukuda, J. Hasegawa, M. Ishida, T. Nakajima, Y. Honda, O. Kitao, H. Nakai, T. Vreven, J. A. Montgomery Jr., J. E. Peralta, F. Ogliaro, M. J. Bearpark, J. Heyd, E. N. Brothers, K. N. Kudin, V. N. Staroverov, R. Kobayashi, J. Normand, K. Raghavachari, A. P. Rendell, J. C. Burant, S. S. Iyengar, J. Tomasi, M. Cossi, N. Rega, N. J. Millam, M. Klene, J. E. Knox, J. B. Cross, V. Bakken, C. Adamo, J. Jaramillo, R. Gomperts, R. E. Stratmann, O. Yazyev, A. J. Austin, R. Cammi, C. Pomelli, J. W. Ochterski, R. L. Martin, K. Morokuma, V. G. Zakrzewski, G. A. Voth, P. Salvador, J. J. Dannenberg, S. Dapprich, A. D. Daniels, Ö. Farkas, J. B. Foresman, J. V. Ortiz, J. Cioslowski and D. J. Fox, *Journal*, 2009.
61 Y. Inoue, *Chem. Rev.*, 1992, **92**, 741-770.
62 R. L. Klug and R. Burcl, *J. Phys. Chem. A*, 2010, **114**, 6401-6407.
63 J. van Gestel, A. R. A. Palmans, B. Titulaer, J. A. J. M. Vekemans and E. W. Meijer, *J. Am. Chem. Soc.*, 2005, **127**, 5490-5494.
64 X. Li, L. Zhu, S. Duan, Y. Zhao and H. Agren, *Phys. Chem. Chem. Phys.*, 2014, **16**, 23854-23860.
65 J. Kim, J. Lee, W. Y. Kim, H. Kim, S. Lee, H. C. Lee, Y. S. Lee, M. Seo and S. Y. Kim, *Nat. Commun.*, 2015, **6**, 6959.